

## Observation of single-spin Dirac fermions at the graphene/ferromagnet interface

Dmitry Usachov, Alexander V. Fedorov, Mikhail M. Otrokov, Alla Chikina, Oleg Vilkov, Anatoly Petukhov, Artem G Rybkin, Yury M Koroteev, Evgueni V. Chulkov, Vera K. Adamchuk, Alexander Grueneis, Clemens Laubschat, and Denis V Vyalikh

*Nano Lett.*, **Just Accepted Manuscript** • Publication Date (Web): 03 Mar 2015

Downloaded from <http://pubs.acs.org> on March 4, 2015

### Just Accepted

“Just Accepted” manuscripts have been peer-reviewed and accepted for publication. They are posted online prior to technical editing, formatting for publication and author proofing. The American Chemical Society provides “Just Accepted” as a free service to the research community to expedite the dissemination of scientific material as soon as possible after acceptance. “Just Accepted” manuscripts appear in full in PDF format accompanied by an HTML abstract. “Just Accepted” manuscripts have been fully peer reviewed, but should not be considered the official version of record. They are accessible to all readers and citable by the Digital Object Identifier (DOI®). “Just Accepted” is an optional service offered to authors. Therefore, the “Just Accepted” Web site may not include all articles that will be published in the journal. After a manuscript is technically edited and formatted, it will be removed from the “Just Accepted” Web site and published as an ASAP article. Note that technical editing may introduce minor changes to the manuscript text and/or graphics which could affect content, and all legal disclaimers and ethical guidelines that apply to the journal pertain. ACS cannot be held responsible for errors or consequences arising from the use of information contained in these “Just Accepted” manuscripts.



# Observation of single-spin Dirac fermions at the graphene/ferromagnet interface

Dmitry Usachov,<sup>\*,†</sup> Alexander Fedorov,<sup>†,‡,¶</sup> Mikhail M. Otrokov,<sup>§,||</sup> Alla  
Chikina,<sup>†,⊥</sup> Oleg Vilkov,<sup>†</sup> Anatoly Petukhov,<sup>†</sup> Artem G. Rybkin,<sup>†</sup> Yury M.  
Koroteev,<sup>§,#</sup> Evgueni V. Chulkov,<sup>§,||</sup> Vera K. Adamchuk,<sup>†</sup> Alexander Grüneis,<sup>‡</sup>  
Clemens Laubschat,<sup>⊥</sup> and Denis V. Vyalikh<sup>†,⊥</sup>

*St. Petersburg State University, 198504 St. Petersburg, Russia, Physikalisches Institut,  
Universität zu Köln, Zùlpicher Strasse 77, 50937 Köln, Germany, IFW Dresden, P.O. Box  
270116, D-01171 Dresden, Germany, Tomsk State University, Lenina Av., 36, 634050  
Tomsk, Russia, Donostia International Physics Center (DIPC), Departamento de Fisica de  
Materiales and CFM-MPC UPV/EHU, 20080 San Sebastian, Spain, Institute of Solid  
State Physics, Dresden University of Technology, D-01062 Dresden, Germany, and  
Institute of Strength Physics and Materials Science of Siberian Branch Russian Academy of  
Sciences, pr. Akademicheskii, 2/4, 634021 Tomsk, Russia*

E-mail: usachov.d@gmail.com

## Abstract

\*To whom correspondence should be addressed

<sup>†</sup>St. Petersburg State University

<sup>‡</sup>University of Köln

<sup>¶</sup>IFW Dresden

<sup>§</sup>Tomsk State University

<sup>||</sup>DIPC Spain

<sup>⊥</sup>Dresden University of Technology

<sup>#</sup>ISPMS SB RAS

1  
2  
3  
4  
5  
6  
7  
8  
9  
10  
11  
12  
13  
14  
15  
16  
17  
18  
19  
20  
21  
22  
23  
24  
25  
26  
27  
28  
29  
30  
31  
32  
33  
34  
35  
36  
37  
38  
39  
40  
41  
42  
43  
44  
45  
46  
47  
48  
49  
50  
51  
52  
53  
54  
55  
56  
57  
58  
59  
60

With the discovery and first characterization of graphene, its potential for spintronic applications was recognized immediately. Since then an active field of research has developed trying to overcome the practical hurdles. One of the most severe challenges is to find appropriate interfaces between graphene and ferromagnetic layers, which are granting efficient injection of spin-polarized electrons. Here we show that graphene grown under appropriate conditions on Co(0001) demonstrates perfect structural properties, and simultaneously exhibits highly spin-polarized charge carriers. The latter was conclusively proven by observation of a single-spin Dirac cone near the Fermi level. This was accomplished experimentally using spin- and angle-resolved photoelectron spectroscopy, and theoretically with density functional calculations. Our results demonstrate that the graphene/Co(0001) system represents an interesting candidate for applications in devices using the spin degree of freedom.

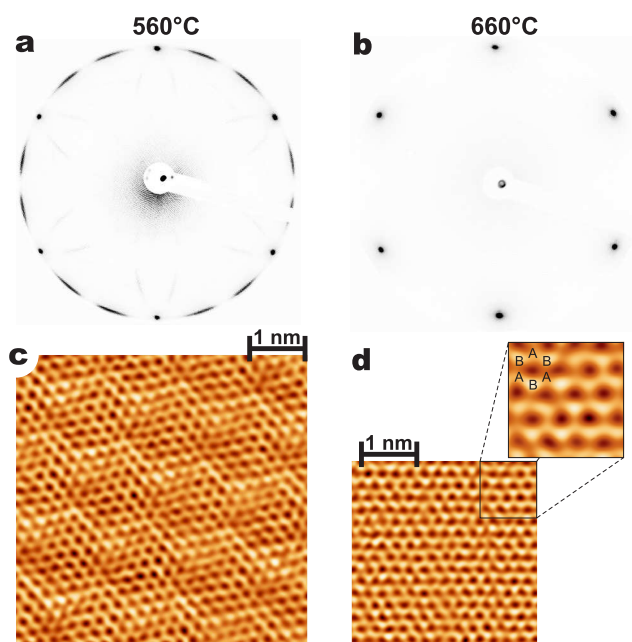
KEYWORDS: Graphene, spin polarization, electronic structure, Dirac cone, spin-resolved ARPES

The most unique properties of the intrinsically two-dimensional material graphene stem from its cone-like dispersion of charge carriers near the Fermi level,  $E_F$ , where electron and hole pockets meet only at the  $\bar{K}$  points of the Brillouin zone.<sup>1</sup> As a consequence the carriers in graphene effectively behave as relativistic Dirac fermions with zero effective mass. This is evidenced, for instance, by their outstanding mobility, which is observed in transport measurements.<sup>2</sup> This behavior opens up significant possibilities for use in next generation electronics,<sup>3</sup> where the spin-degree of freedom in particular might be used.<sup>4,5</sup> However, graphene's unique electronic structure becomes strongly altered when brought into contact with ferromagnetic metals, which are used as spin-polarizing substrates.<sup>6,7</sup> For any practical use it is therefore necessary to find an appropriate graphene/ferromagnet system where the remarkable properties of graphene and, in particular, its cone-like dispersion near the Fermi level are preserved.

1  
2  
3  
4 Numerous studies of the electronic band structure of graphene/metal systems show that  
5 due to the strong interaction between C  $2p_z$  and  $d$  states of the metallic substrate, the  $\pi$ -states  
6 of graphene are essentially modified and largely shifted away from  $E_F$ . For example, this has  
7 been shown for several metals, which are characterized by an open and chemically active  $d$ -  
8 shell, as is the case for Ni, Co, Fe, Rh, Re, and Ru.<sup>8-17</sup> Only in the cases of weakly interacting  
9 substrates does the Dirac cone remain almost undisturbed. This is predicted theoretically<sup>7</sup>  
10 and observed experimentally in graphene on Au, Cu, Ir, Pt, Al and on silicides, where  
11 the Dirac point is close to  $E_F$ .<sup>10,16,18-22</sup> For the cases of magnetically interesting substrates  
12 like Ni(111) and Co(0001), the Dirac cone is modified in a very special way. It is split in  
13 several parts, which retain some similarities to the Dirac cone of freestanding graphene. The  
14 main part was identified in photoemission experiments as a gapless Dirac cone with its apex  
15 located at the binding energy of about 2.8 eV.<sup>14</sup> According to theoretical calculations the  
16 states close to the apex are notably mixed with metal  $3d$  states.<sup>14,15,23</sup> This mixing destroys  
17 the conical band above the energy of 2 eV. Thus far, no ferromagnetic substrate is known  
18 where the electronic structure of free-standing graphene is widely conserved. Interestingly,  
19 theoretical considerations suggest that in spite of strong distortions of the linear dispersion  
20 of the  $\pi$ -states due to their hybridization with metal  $d$ -states, a new spin-polarized cone-like  
21 interface band near the Fermi level might exist.<sup>6,7,14,15,23-25</sup> This offers an opportunity to  
22 obtain desired electronic and magnetic properties, and combine them in these composite  
23 structures.  
24  
25  
26  
27  
28  
29  
30  
31  
32  
33  
34  
35  
36  
37  
38  
39  
40  
41  
42  
43

44 Here, for the first time we experimentally demonstrate and theoretically support that  
45 such a Dirac-cone-like feature exists in a graphene/ferromagnet system, with its apex close  
46 to  $E_F$ . Studying a perfectly oriented graphene/Co(0001) system by spin- and angle-resolved  
47 photoelectron spectroscopy (SR-ARPES) we found that this cone-like band is formed by  
48 states with only one spin orientation. A system with such a property could act as a source of  
49 spin-polarized current, which is one of the main components of spintronic devices. The key  
50 aspect that gives rise to these properties is the perfect mutual orientation of the graphene  
51  
52  
53  
54  
55  
56  
57  
58  
59  
60

1  
2  
3  
4 layer and the Co(0001) substrate, which may be achieved following the appropriate growth  
5  
6 protocol.



7  
8  
9  
10  
11  
12  
13  
14  
15  
16  
17  
18  
19  
20  
21  
22  
23  
24  
25  
26  
27  
28  
29  
30  
31  
32  
33  
34  
35  
36  
37  
38  
39  
40  
41  
42  
43  
44  
45  
46  
47  
48  
49  
50  
51  
52  
53  
54  
55  
56  
57  
58  
59  
60  
Figure 1: Graphene structure in real and reciprocal space. LEED patterns of graphene/Co(0001) for (a) misoriented graphene domains, and (b) perfectly oriented graphene. The electron energy was 70 eV. Respective STM images for (c) misoriented domain, rotated by  $\sim 10^\circ$  relative to the Co(0001) lattice and (d) graphene aligned in a registry with the substrate. The horizontal direction is parallel to the  $[11\bar{2}0]$  direction of cobalt. The inset shows a zoomed region manifesting non-equivalence of two sublattices. The synthesis temperature is shown above the images.

**Structural properties of graphene/Co interface.** We explored the structural properties of a single graphene layer grown by chemical vapor deposition (CVD) on a layer of Co(0001) and discovered that the highly ordered graphene perfectly oriented with respect to the substrate could be grown only within a certain temperature range. As an example, in Figure 1 we show the results of low energy electron diffraction (LEED) and scanning tunneling microscopy (STM) characterization of graphene on Co(0001) prepared at the temperature of  $560^\circ\text{C}$  (Fig. 1a,c), as well as at  $660^\circ\text{C}$  (Fig. 1b,d). The latter is essentially quite high, and close to its destruction temperature. The system prepared at the lower temperature is characterized in LEED by the arc shaped reflexes (Fig. 1a). This observation implies the presence of predominant misoriented domains, the existence of which has been established

1  
2  
3 by other studies.<sup>11,13,14</sup> The STM data taken from the system are consistent with the LEED  
4 results. They demonstrate a well-known moiré pattern, which is intrinsic to the mismatched  
5 interface (Fig. 1c).  
6  
7  
8

9  
10 Next, we looked closely at the LEED and STM data taken for the second system (Fig. 1b  
11 and 1d), which was prepared at high temperature. In this case we can safely conclude that  
12 carbon atoms, packed into the graphene matrix, perfectly fit the lattice of the underlying  
13 cobalt layer. This is possible because the misfit between lattice parameters of free graphene  
14 and cobalt is less than 2%. LEED shows a  $(1 \times 1)$  structure and the STM image demonstrates  
15 a three-fold symmetry of the system, which indicates the nonequivalence of the two carbon  
16 sublattices A and B, depicted in inset in Fig. 1d. This may correspond to the structure,  
17 in which the atoms of one sublattice are located above Co atoms, while the others occupy  
18 hollow sites.  
19  
20  
21  
22  
23  
24  
25  
26  
27

28 It should be noted that recently the formation of graphene/Co(0001) interface with  $(1 \times 1)$   
29 LEED pattern was demonstrated on the Co film with the thickness of 3 nm at the growth  
30 temperature of 430°C.<sup>26</sup> This suggests that the synthesis temperature may be not the decisive  
31 parameter, which ensures perfect graphene orientation. In our experiments much thicker Co  
32 films were used (not thinner than 10 nm), which was necessary for keeping the film integrity  
33 at the synthesis temperatures up to 660°C. We suppose that thicker Co films may require  
34 annealing at higher temperature in order to reach good crystallization, which is important  
35 for graphene ordering. Also the type of hydrocarbon gas used in CVD may be important.  
36 Interestingly, despite the perfect graphene orientation no spin-polarized interface state was  
37 detected in Ref. 26. This indicates certain structural differences between the systems formed  
38 at different conditions. The possible difference, which may be not reflected in the LEED  
39 pattern, is a presence of nonperiodic imperfections of the graphene/Co interface, formed at  
40 low temperature. In the case of Ni(111) it has been demonstrated that the quality of graphene  
41 is increasing with the synthesis temperature.<sup>27</sup> Graphene grown at the temperatures of 400–  
42 450°C is characterized by a high concentration of defects, while at 650°C a high-quality  
43  
44  
45  
46  
47  
48  
49  
50  
51  
52  
53  
54  
55  
56  
57  
58  
59  
60

lattice is formed.<sup>27</sup> For this reason we avoided low growth temperatures and used STM for proving the high graphene quality.

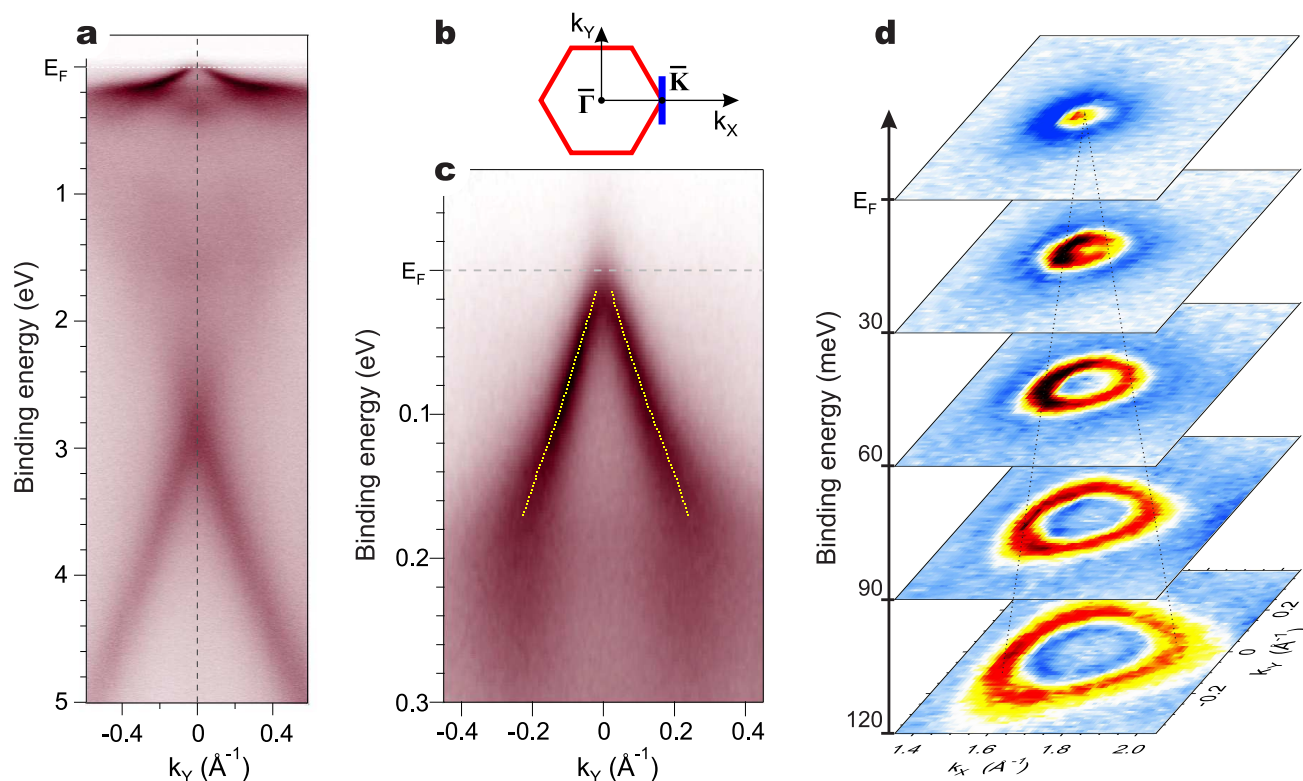


Figure 2: ARPES insight into the electronic structure of graphene/Co interface. (a) ARPES data taken near the  $\bar{K}$ -point from well-oriented graphene on Co(0001) at room temperature, using 40 eV photons with  $s + p$  polarization. (b) Structure of graphene in momentum space; the line schematically indicates the direction of measurements. (c) ARPES insight into the mini cone at  $E_F$  obtained with 28 eV photons. (d) ARPES constant-energy maps of the mini cone.

**Electronic structure viewed by ARPES.** The electronic structure of this perfectly oriented graphene on Co(0001) was next explored in detail by spin- and angle- resolved photoelectron spectroscopy. In Fig. 2a we present ARPES spectra taken at the  $\bar{K}$ -point of the surface Brillouin zone (BZ) (the data at the  $\bar{\Gamma}$ -point are shown in Fig. S3a in Supporting Info). Figure 2b schematically shows the BZ of graphene, and the direction of the ARPES measurements. Looking at the ARPES-derived band maps, two interesting features may be seen: (i) the main Dirac cone,<sup>14</sup> which is shifted to  $\sim 2.8$  eV below  $E_F$ , and (ii) another cone-like feature near  $E_F$ . The latter is shown magnified in Fig. 2c, where the Fermi level

1  
2  
3  
4 approaching is clearly visible. The dispersion of this state does not depend on the photon  
5 energy and its photoemission intensity is relatively high in the range of  $h\nu = 22 - 60$  eV.  
6  
7 To prove this spectral feature has an intrinsic conical shape, representing carriers with the  
8 properties of Dirac fermions, we took several constant energy maps. These are joined together  
9  
10 in Fig. 2d. Obviously, the ARPES data reveal trigonally warped contours of the discussed  
11 “mini cone” feature, demonstrating certain similarity to the Dirac cone of quasi-freestanding  
12 graphene.<sup>10</sup> The photoemission intensity distribution is not symmetric, demonstrating higher  
13 intensity in the first BZ. However, the asymmetry is not so pronounced as in the case of main  
14 Dirac cone (see Fig. S4 in Supporting Info). This difference can be explained by a significant  
15 contribution of cobalt *d*-orbitals to the cone-like interface state. It should be noted that the  
16 dotted lines in Fig. 2c show the result of fitting of momentum distribution curves with two  
17 lorentzian peak functions. These lines show the band dispersion, which appears almost linear  
18 in the energy range of 30 – 150 meV; however the fit result is not well defined at the  $\bar{K}$ -point,  
19 where the two peaks become strongly overlapped. Thus the exact shape of the cone apex  
20 cannot be reliably determined from experimental data. However, we can definitely conclude  
21 that the energy distance between the band and the Fermi level is smaller than the energy of  
22 thermal excitations at the room temperature (26 meV).  
23  
24  
25  
26  
27  
28  
29  
30  
31  
32  
33  
34  
35  
36  
37

38 As we see, the mini cone feature is localized within a narrow energy region,  $\sim 0.2$  eV below  
39 the  $E_F$ . The slope of the linear part of the band, which is often identified with a Fermi velocity  
40  $v_F$ , is nearly ten times smaller than that observed in a free-standing graphene. The reduced  
41  $v_F$  in the graphene/Co(0001) system reflects a certain influence of the “heavy” *d*-electrons  
42 of the cobalt substrate. This suggests that the mini cone contains notable contribution of  
43 *3d* states of cobalt hybridized with *2p* states of carbon.  
44  
45  
46  
47  
48  
49

50 **The nature of the mini Dirac cone.** For deeper understanding of the observed band  
51 structure we carried out *ab initio* calculations. Taking into account sublattice asymmetry,  
52 observed in STM images, we considered a *top-fcc* adsorption geometry, which we have found  
53 to be slightly more favorable energetically (by only 6 meV per C atom) than the *top-hcp*  
54  
55  
56  
57  
58  
59  
60

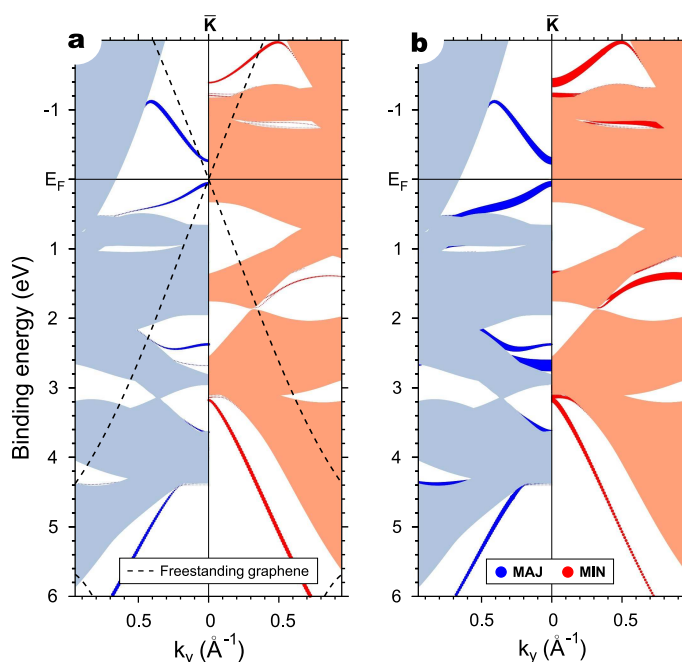


Figure 3: Theoretical insight into surface and bulk spin-resolved band structure of graphene/Co(0001). Size of spots is proportional to the contribution of carbon (a) and upper cobalt layer atoms (b) to the wave function. The dashed line shows the bands of freestanding graphene. Shaded bands correspond to projected bulk Co states. The path in the  $\mathbf{k}$ -space corresponds to the experiment geometry, shown in Fig. 2b.

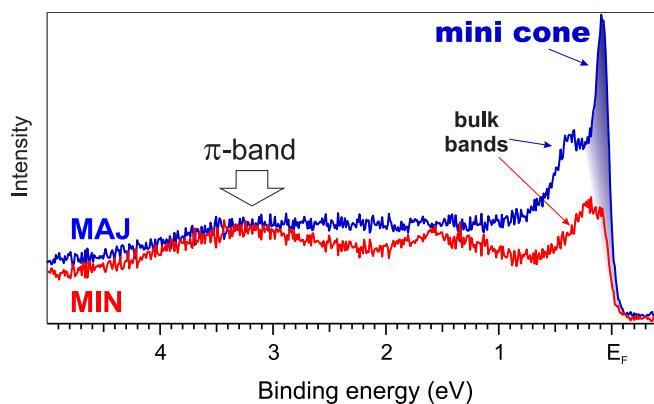


Figure 4: Spin-resolved ARPES view of the mini cone feature. The spectra were taken at the  $\bar{\mathbf{K}}$ -point of the BZ along the vertical dashed line in Fig. 2a. Momentum resolution was  $\sim 0.2\text{\AA}^{-1}$ ,  $h\nu = 37\text{ eV}$ . The sample was magnetized along the  $\bar{\Gamma\mathbf{K}}$  direction. Magnetization along the  $\bar{\Gamma\mathbf{M}}$  direction results in the similar SR-ARPES spectra.

1  
2  
3 structure. The ferromagnetic nature of Co results in exchange splitting of all the states  
4 within the graphene/Co(0001) system, and formation of the majority and minority states.  
5  
6 When the freestanding graphene starts to interact with the Co substrate, the spin-up and  
7 spin-down states of the initially degenerate Dirac cone (dashed line in Fig. 3a) are coupled  
8 differently with the respective spin-polarized Co states. The apex of the unperturbed Dirac  
9 cone falls directly into the local energy gap of the bulk majority states of Co. Therefore, the  
10 conical dispersion of spin-up states is mainly preserved near the cone apex. The interplay  
11 with cobalt bands only leads to the opening of a small gap of  $\sim 0.33$  eV at the  $E_F$  and  
12 reducing the velocity of quasiparticles. This scenario explains the mini cone formation (see  
13 Fig. S1 in Supporting Information). The spin-down Dirac cone apex strongly overlaps with  
14 the bulk projected Co minority states near  $E_F$ , and their interaction pushes the lower cone  
15 apex down, leading to a huge splitting of  $\sim 4.5$  eV in the  $\pi$ -band. It should be noted that  
16 in Ref. 14 the formation of a second Dirac cone was described theoretically and discussed in  
17 detail for the case of graphene/Ni(111) system. It was emphasized that the second cone at  
18 the  $E_F$  is a counterpart of the main Dirac cone with its apex at 2.8 eV.  
19  
20  
21  
22  
23  
24  
25  
26  
27  
28  
29  
30  
31  
32  
33

34 The mini cone states are formed by the mixture of C  $2p_z$  and Co  $3d$  states. They  
35 have an intrinsically two-dimensional nature and their wave-functions are spatially located  
36 at the interface (see Fig. S2 in Supporting Info). This theoretical finding is conclusively  
37 confirmed by the absence of the  $k_z$  dispersion of the mini cone feature in ARPES spectra.  
38 The mini cone appears only in the majority spin bands, and therefore it can be considered  
39 as a 100% spin-polarized interface state. It should be noted that the ARPES data revealed  
40 an extensive region of linearity of the mini cone dispersion, therefore it may be considered  
41 as a Dirac cone. The calculation demonstrates that the cone apex is parabolic due to  
42 presence of a gap. It implies that Dirac fermions are not massless. The gap originates  
43 from graphene symmetry breaking in the *top-fcc* configuration and may vanish in a more  
44 symmetric *bridge-top* structure, as it was predicted for the graphene/Ni(111) system.<sup>25</sup> Since  
45 the upper unoccupied part of the mini cone is not accessible with ARPES, we are not able  
46  
47  
48  
49  
50  
51  
52  
53  
54  
55  
56  
57  
58  
59  
60

1  
2  
3  
4 to determine reliably which adsorption geometry was realized in experiment.

5  
6 The predicted strong spin polarization of the mini cone is experimentally confirmed by  
7  
8 the SR-ARPES data shown in Fig. 4. The spectrum was taken along a cut through the  
9  
10  $\bar{\mathbf{K}}$ -point. The majority spin channel exhibits a strong peak just below  $E_F$ , while no peak is  
11  
12 present in the minority spin signal. The peak in the majority channel reflects the highly spin-  
13  
14 polarized mini cone located in the spin-projected band gap of the Co substrate. Two bumps  
15  
16 seen at 0.2 and 0.35 eV in the minority and majority spectra, respectively, we attribute  
17  
18 to the edges of bulk cobalt bands with high density of states. This is consistent with our  
19  
20 calculation within the accuracy of DFT. A broad peak in the minority-spin signal at  $\sim 3.2$  eV  
21  
22 is related to the spin-polarized apex of the main Dirac cone, in agreement with the results of  
23  
24 our calculation. The peak is broadened and shifted to higher binding energies (with respect  
25  
26 to the data shown in Fig. 2a) due to lower momentum resolution in spin-resolved mode.

27  
28 In summary, the presented data clearly demonstrate the existence of a single-spin mini  
29  
30 Dirac cone at  $E_F$  when the graphene monolayer is perfectly oriented on a Co(0001) surface.  
31  
32 It is important to emphasize that those graphene/Co(0001) samples which mainly consist of  
33  
34 misoriented domains DO NOT reveal this mini cone feature (see Fig. S3b). The intensity  
35  
36 of the mini cone is proportional to the fraction of domains with  $(1 \times 1)$  structure, which  
37  
38 we believe is why the mini cone was not detected and described in the previous studies. It  
39  
40 should be noted that according to calculations, the band structure of the graphene/Ni(111)  
41  
42 interface is very similar to that of graphene/Co(0001). A spin-polarized mini cone at the  $E_F$   
43  
44 was predicted for this system, too.<sup>14</sup> It can be identified in the calculated band structure of  
45  
46 graphene/Ni(111) system.<sup>7,14,16,24,25</sup> The epitaxial properties of the Ni-based system are more  
47  
48 favorable, and the  $(1 \times 1)$  structure is usually formed due to a perfect match of the lattice  
49  
50 constants. Nevertheless, the experimental observation of a mini cone in this system has been  
51  
52 never reported. We have carefully measured ARPES spectra of graphene/Ni(111) interface  
53  
54 and found that the mini cone appears in this system as well (see Fig. S5 in Supporting Info).  
55  
56 However, the feature is not as striking and pronounced as is seen in the case of the Co-system.  
57  
58  
59  
60

1  
2  
3  
4 It seems from the data that the mini cone apex is located below the  $E_F$  and its upper part is  
5 visible, implying that the gap is very small ( $< 40$  meV) or absent. According to the recent  
6 calculations<sup>25</sup> such gap corresponds to a *bridge-top* adsorption geometry, in which the upper  
7 metal layer does not break the symmetry of the graphene lattice. In the symmetry-breaking  
8 configurations like *top-fcc* or *top-hcp* the gap is expected to reach 0.5 eV.<sup>25</sup> This may indicate  
9 that in our sample the *bridge-top* geometry was dominating. However, the data in Fig. S5  
10 must be interpreted with a great caution, because the mini cone falls into the region with  
11 high density of Ni 3d minority states, which also contribute to the ARPES intensity and may  
12 mask the real dispersion of the interface state. Our finding together with the results of band  
13 structure calculations for multiple strongly bound graphene systems<sup>7,14,16,24,25,28</sup> implies that  
14 the mini cone formation is a quite general feature of graphene interfacing with *d*-metals.  
15  
16  
17  
18  
19  
20  
21  
22  
23  
24

25  
26 The contact of graphene with a ferromagnetic material like Co or Ni can be a source  
27 of spin-polarized electrons and, therefore, is a very promising system for spintronic de-  
28 vices.<sup>4,6,11,16,29,30</sup> Our results clearly demonstrate that the use of an epitaxial graphene/Co  
29 interface might be more efficient than the use of polycrystalline metal electrodes. This sys-  
30 tem has a unique electronic structure near the Fermi level – a single-spin interface state  
31 at the  $\bar{K}$ -point of the BZ. The notable contribution of graphene  $\pi$ -orbitals to this state  
32 accounts for a good coupling between the wave function of spin and charge carriers at the  
33 interface and the wave function in freestanding graphene when it is used as a conducting  
34 channel between electrodes. We believe that this can provide good conditions for effective  
35 spin-polarized transport, in agreement with theoretical predictions.<sup>30</sup>  
36  
37  
38  
39  
40  
41  
42  
43  
44  
45  
46  
47  
48

49 **Methods.** The clean Co(0001) surface was obtained by growing the crystalline cobalt  
50 film with a thickness of 10 nm on the clean W(110) substrate in ultra-high vacuum (UHV) at  
51 a deposition rate of 1.5 Å/min at the room temperature. Graphene film was synthesized in  
52 the UHV chamber using chemical vapour deposition (CVD) by exposing the heated sample  
53 surface to propylene at a pressure of  $10^{-6}$  mbar and a temperature of 560-660°C for 15 min.  
54  
55  
56  
57  
58  
59  
60

1  
2  
3  
4  
5  
6  
7  
8  
9  
10  
11  
12  
13  
14  
15  
16  
17  
18  
19  
20  
21  
22  
23  
24  
25  
26  
27  
28  
29  
30  
31  
32  
33  
34  
35  
36  
37  
38  
39  
40  
41  
42  
43  
44  
45  
46  
47  
48  
49  
50  
51  
52  
53  
54  
55  
56  
57  
58  
59  
60

At these conditions the synthesis reaction is self-limiting. The growth starts immediately on a hot catalytically active metal surface and proceeds until the surface is covered by a single graphene layer.<sup>11,14,22</sup> No further growth is possible on such graphene-passivated surface, therefore the synthesis always results in the formation of a complete graphene single monolayer. Monolayer graphene thickness was proved by X-ray photoemission spectroscopy using the intensity ratio of measured C 1s and Co(Ni) 3p lines. Depending on the synthesis temperature, different ordering of graphene domains was obtained. A similar procedure was used to form graphene on the Ni(111) surface.<sup>31,32</sup>

Spin- and angle-resolved photoemission spectroscopy (SARPES and ARPES) was performed at the UE-112 PGM-1 beamline at BESSY II synchrotron radiation facility using RGBL-2 station. All measurements were done using linearly polarized radiation. Spin-resolved spectra were obtained from the data acquired in two opposite sample magnetization directions in order to eliminate spectrometer asymmetry.<sup>33</sup> No smoothing was applied to the data.

Scanning tunneling microscopy (STM) images were obtained using Omicron VT SPM in the research resource center “Physical Methods of Surface Investigation” of St. Petersburg State University (SPbSU), where perfectly oriented graphene was synthesized on Co(0001) for the first time. The hexagonal close-packed crystal structure of cobalt film was confirmed after graphene synthesis using Bruker “D8 DISCOVER” X-ray diffractometer in the resource center for X-ray Diffraction Studies of SPbSU.

We carried out *ab initio* electronic structure calculations of graphene/Co(0001) using the projector augmented-wave method<sup>34</sup> as implemented in the VASP code.<sup>35,36</sup> The generalized gradient approximation to the exchange-correlation potential in the revised Perdew-Burke-Ernzerhof version (PBEsol)<sup>37</sup> was employed.

The system was simulated using the 19-layer-thick Co film with a graphene monolayer attached to both its sides. The lateral lattice parameter was fixed as in the experiment for bulk Co,  $a=2.507\text{\AA}$ . All the atomic layers in the supercell, including graphene ones, were

1  
2  
3 relaxed until the forces on each atom were less than  $10^{-2}$  eV/Å. The energy cutoff for the  
4 plane-wave expansion of wave functions was set to 400 eV, and a **k**-point grid of  $12 \times 12 \times 1$   
5 was used to sample the two-dimensional Brillouin zone.  
6  
7  
8  
9

### 10 11 **Supporting Information Available:**

12 Detailed results of the DFT calculations of graphene/Co(0001) system and SR-ARPES data  
13 for graphene/Ni(111) system are presented. This material is available free of charge via the  
14 Internet at <http://pubs.acs.org>.  
15  
16  
17  
18  
19

### 20 21 **Acknowledgement**

22 The authors acknowledge Saint-Petersburg State University for a research grants  
23 11.37.634.2013 and 11.50.202.2015, RFBR (grant No. 14-02-31150), and BMBF (grant No.  
24 05K12OD3). A.G. acknowledges support from the ERC grant Super2D. M.M.O. and E.V.C  
25 acknowledge the financial support of the University of Basque Country UPV/EHU (Grant  
26 No. GIC07-IT-756-13) as well as of the Departamento de Educacion del Gobierno Vasco  
27 and the Spanish Ministerio de Ciencia e Innovacion (Grant No. FIS2010-19609-C02-01).  
28 We acknowledge Helmholtz Zentrum Berlin für Materialien und Energie for support within  
29 bilateral Russian-German Laboratory program. We cordially thank Dr. Allison L. Stelling  
30 for editing the manuscript.  
31  
32  
33  
34  
35  
36  
37  
38  
39  
40  
41  
42  
43  
44

### 45 **References**

- 46  
47 (1) Neto, A. H. C.; Guinea, F.; Peres, N. M. R.; Novoselov, K. S.; Geim, A. K. *Rev. Mod.*  
48 *Phys.* **2008**, *81*, 109–162.  
49  
50  
51  
52 (2) Das Sarma, S.; Adam, S.; Hwang, E. H.; Rossi, E. *Rev. Mod. Phys.* **2011**, *83*, 407–470.  
53  
54  
55 (3) Avouris, P.; Dimitrakopoulos, C. *Mater. Today* **2012**, *15*, 86–97.  
56  
57  
58  
59  
60

- 1  
2  
3  
4  
5  
6  
7  
8  
9  
10  
11  
12  
13  
14  
15  
16  
17  
18  
19  
20  
21  
22  
23  
24  
25  
26  
27  
28  
29  
30  
31  
32  
33  
34  
35  
36  
37  
38  
39  
40  
41  
42  
43  
44  
45  
46  
47  
48  
49  
50  
51  
52  
53  
54  
55  
56  
57  
58  
59  
60
- (4) Hill, E. W.; Novoselov, A. K.; Schedin, K.; Blake, P. *IEEE Trans. Magn.* **2006**, *42*, 2694–2696.
- (5) Tombros, N.; Jozsa, C.; Popinciuc, M.; Jonkman, H. T.; van Wees, B. J. *Nature* **2007**, *448*, 571–U4.
- (6) Karpan, V. M.; Giovannetti, G.; Khomyakov, P. A.; Talanana, M.; Starikov, A. A.; Zwierzycki, M.; van den Brink, J.; Brocks, G.; Kelly, P. J. *Phys. Rev. Lett.* **2007**, *99*, 176602.
- (7) Khomyakov, P. A.; Giovannetti, G.; Rusu, P. C.; Brocks, G.; van den Brink, J.; Kelly, P. J. *Phys. Rev. B* **2009**, *79*, 195425.
- (8) Nagashima, A.; Tejima, N.; Oshima, C. *Phys. Rev. B* **1994**, *50*, 17487–17495.
- (9) Dedkov, Y. S.; Shikin, A. M.; Adamchuk, V. K.; Molodtsov, S. L.; Laubschat, C.; Bauer, A.; Kaindl, G. *Phys. Rev. B* **2001**, *64*, 035405.
- (10) Varykhalov, A.; Sánchez-Barriga, J.; Shikin, A. M.; Biswas, C.; Vescovo, E.; Rybkin, A.; Marchenko, D.; Rader, O. *Phys. Rev. Lett.* **2008**, *101*, 157601.
- (11) Varykhalov, A.; Rader, O. *Phys. Rev. B* **2009**, *80*, 035437.
- (12) Brugger, T.; Günther, S.; Wang, B.; Dil, J. H.; Bocquet, M.-L.; Osterwalder, J.; Winterlin, J.; Greber, T. *Phys. Rev. B* **2009**, *79*, 045407.
- (13) Sánchez-Barriga, J.; Varykhalov, A.; Scholz, M.; Rader, O.; Marchenko, D.; Rybkin, A.; Shikin, A.; Vescovo, E. *Diam. Relat. Mater.* **2010**, *19*, 734–741.
- (14) Varykhalov, A.; Marchenko, D.; Sánchez-Barriga, J.; Scholz, M. R.; Verberck, B.; Trauzettel, B.; Wehling, T. O.; Carbone, C.; Rader, O. *Phys. Rev. X* **2012**, *2*, 041017.
- (15) Voloshina, E.; Dedkov, Y. *Phys. Chem. Chem. Phys.* **2012**, *14*, 13502–13514.
- (16) Generalov, A.; Voloshina, E.; Dedkov, Y. *Appl. Surf. Sci.* **2013**, *267*, 8–11.

- 1  
2  
3  
4 (17) Papagno, M.; Moras, P.; Sheverdyeva, P. M.; Doppler, J.; Garhofer, A.; Mittendorfer, F.; Redinger, J.; Carbone, C. *Phys. Rev. B* **2013**, *88*, 235430.  
5  
6  
7  
8  
9 (18) Pletikosić, I.; Kralj, M.; Pervan, P.; Brako, R.; Coraux, J.; N'Diaye, A. T.; Busse, C.;  
10 Michely, T. *Phys. Rev. Lett.* **2009**, *102*, 056808.  
11  
12  
13 (19) Sutter, P.; Sadowski, J. T.; Sutter, E. *Phys. Rev. B* **2009**, *80*, 245411.  
14  
15  
16 (20) Starodub, E.; Bostwick, A.; Moreschini, L.; Nie, S.; Gabaly, F. E.; McCarty, K. F.;  
17 Rotenberg, E. *Phys. Rev. B* **2011**, *83*, 125428.  
18  
19  
20 (21) Rybkina, A. A.; Rybkin, A. G.; Fedorov, A. V.; Usachov, D. Y.; Yachmenev, M. E.;  
21 Marchenko, D. E.; Vilkov, O. Y.; Nelyubov, A. V.; Adamchuk, V. K.; Shikin, A. M.  
22 *Surf. Sci.* **2013**, *609*, 7–17.  
23  
24  
25 (22) Vilkov, O.; Fedorov, A.; Usachov, D.; Yashina, L. V.; Generalov, A. V.; Borygina, K.;  
26 Verbitskiy, N. I.; Grüneis, A.; Vyalikh, D. V. *Sci. Reports* **2013**, *3*, 2168.  
27  
28  
29 (23) Eom, D.; Prezzi, D.; Rim, K. T.; Zhou, H.; Lefenfeld, M.; Xiao, S.; Nuckolls, C.;  
30 Hybertsen, M. S.; Heinz, T. F.; Flynn, G. W. *Nano Lett.* **2009**, *9*, 2844–2848.  
31  
32  
33 (24) Garcia-Lekue, A.; Balashov, T.; Olle, M.; Ceballos, G.; Arnau, A.; Gambardella, P.;  
34 Sanchez-Portal, D.; Mugarza, A. *Phys. Rev. Lett.* **2014**, *112*, 066802.  
35  
36  
37 (25) Zhang, W.-B.; Chen, C.; Tang, P.-Y. *J. Chem. Phys.* **2014**, *141*, 044708.  
38  
39  
40 (26) Pacilé, D.; Lisi, S.; Di Bernardo, I.; Papagno, M.; Ferrari, L.; Pisarra, M.; Caputo, M.;  
41 Mahatha, S. K.; Sheverdyeva, P. M.; Moras, P.; Lacovig, P.; Lizzit, S.; Baraldi, A.;  
42 Betti, M. G.; Carbone, C. *Phys. Rev. B* **2014**, *90*, 195446.  
43  
44  
45 (27) Jacobson, P.; Stöger, B.; Garhofer, A.; Parkinson, G. S.; Schmid, M.; Caudillo, R.;  
46 Mittendorfer, F.; Redinger, J.; Diebold, U. *J. Phys. Chem. Lett.* **2012**, *3*, 136–139.  
47  
48  
49  
50  
51  
52  
53  
54  
55  
56  
57  
58  
59  
60

- 1  
2  
3  
4 (28) Li, Y.; Chen, P.; Zhou, G.; Li, J.; Wu, J.; Gu, B.-L.; Zhang, S. B.; Duan, W. *Phys.*  
5  
6 *Rev. Lett.* **2012**, *109*, 206802.  
7  
8 (29) Dedkov, Y. S.; Fonin, M.; Laubschat, C. *Appl. Phys. Lett.* **2008**, *92*, 052506.  
9  
10 (30) Cho, Y.; Choi, Y. C.; Kim, K. S. *J. Phys. Chem. C* **2011**, *115*, 6019–6023.  
11  
12 (31) Oshima, C.; Nagashima, A. *J. Phys.: Condens. Matter* **1997**, *9*, 1–20.  
13  
14 (32) Grüneis, A.; Kummer, K.; Vyalikh, D. V. *New J. Phys.* **2009**, *11*, 073050.  
15  
16 (33) Johnson, P. *Rep. Prog. Phys.* **1997**, *60*, 1217–1304.  
17  
18 (34) Blöchl, P. E. *Phys. Rev. B* **1994**, *50*, 17953–17979.  
19  
20 (35) Kresse, G.; Furthmüller, J. *Phys. Rev. B* **1996**, *54*, 11169–11186.  
21  
22 (36) Kresse, G.; Joubert, D. *Phys. Rev. B* **1999**, *59*, 1758–1775.  
23  
24 (37) Perdew, J. P.; Ruzsinszky, A.; Csonka, G. I.; Vydrov, O. A.; Scuseria, G. E.; Con-  
25  
26  
27  
28  
29  
30  
31  
32  
33  
34  
35  
36  
37  
38  
39  
40  
41  
42  
43  
44  
45  
46  
47  
48  
49  
50  
51  
52  
53  
54  
55  
56  
57  
58  
59  
60

**mini Dirac cone**

